Analysis of calcium dynamics for dim-light responses in rod and cone photoreceptors.

Annia Abtout and Jürgen Reingruber

Abstract

Rod and cone photoreceptors in vertebrate eyes are fundamental sensory neurons underlying vision. They use a sophisticated signal transduction pathway consisting of a series of biochemical processes to convert the absorption of light into an electrical response. Several of these processes are modulated by feedback mechanisms that depend on the intracellular Ca^{2+} concentration. In this work we use a representative phototransduction model with fast buffering to study how the Ca^{2+} dynamics affects the light response of mouse rod and cone photoreceptors. We obtain analytic solutions for dim-light stimulation that reveal how the dynamics of the Ca^{2+} concentration and the electrical current are correlated. We show how modifying the Ca^{2+} dynamics via buffering affects amplitude and waveform of flash and step responses. We infer that under normal physiological conditions the change in the Ca^{2+} concentration is proportional to the current. We show that damped oscillations appear if the Ca^{2+} dynamics becomes slowed down and delayed with respect to the current, e.g. through the application of buffers. We find that oscillations do not require the presence of slow buffers. We show that the phase space of the dim-light response is controlled by the ratio between the effective rate μ_{ca} that controls the Ca^{2+} dynamics, and the dark turnover rate of cyclic GMP β_d. Finally, we investigate how the light response is affected by modifying the extracellular Ca^{2+} concentration. In summary, we provide a comprehensive analysis that reveals how the Ca^{2+} dynamics affects the dim-light response in rods and cones.

Significance

The signal transduction pathway of vertebrate rod and cone photoreceptors transforms light into an electrical response. It is regulated by several feedback processes that depend on the intracellular Ca^{2+} concentration. Despite of the importance of this feedback for the photoreceptor functioning, it is not well studied how modifying the Ca^{2+} dynamics affects the light response, for example by adding buffers. Here we derive analytic results for dim-light stimulations that provide insight into how the Ca^{2+} dynamics and the electrical current response are correlated. Our analysis can be used to infer properties of the Ca^{2+} dynamics from the observed current response, and provides insight if direct measurements of the Ca^{2+} dynamics in the small outer segment of a photoreceptors are not available.

Introduction

In the outer segment of vertebrate rod and cone photoreceptors, a multistep signal transduction pathway transforms the activation of the photopigment by absorption of light into an electrical current response(see e.g. [1, 2, 3, 4]). Light dependent photopigment activation is coupled via a G-protein cascade to the activation of the effector enzyme phosphodiesterase-6 (PDE). The signal encoded by the time course of light-activated PDE is then converted into a current response, because

activated PDE hydrolyses cyclic guanosine monophosphate (cGMP), a second messenger that controls the opening of CNG channels in the outer segment membrane. The light-dependent decline in the cGMP concentration leads to a reduction in the number of open CNG channels and photoreceptor hyperpolarization. The decrease in cGMP concentration produced by hydrolysis of spontaneously activated and light-activated PDE is restored by synthesis of cGMP, catalyzed by guanylyl cyclase.

Many of the biophysical processes that participate in this phototransduction pathway are modulated by Ca^{2+}-feedback, which is important for response termination and light adaptation [5]. Whereas the dynamics of the electrical current is experimentally well characterized, it remains difficult to measure the time course of the change in the free-Ca^{2+} concentration in the constrained space of the outer segment. Recently the Ca^{2+}-dynamics in the relatively large outer segment of amphibian rods (Xenopus frog) has been measured using a fluorescent calcium dye [6]. However, no such data is available that shows the Ca^{2+}-dynamics in the much smaller outer segments of mouse or primate rods, or of cones. As a consequence, it is unclear how exactly the intracellular Ca^{2+} concentration changes during a light response in these photoreceptors, and how it's dynamics affects the electrical current. For example, it has been observed that an increase in intracellular Ca^{2+}-buffering induces oscillations in primate and guinea pig rods [7, 8, 9], mouse rods [8, 10], and toad rods [9]. In primate cones, oscillations have been observed without any manipulation of Ca^{2+} [11, 12, 13]. Moreover, for primate cones it has been observed that oscillations can be removed by lowering the extracellular Ca^{2+} concentration [14]. In absence of direct measurements of the Ca^{2+} concentration in such photoreceptors, modelling provides an indirect means to relate the dynamics of the change in Ca^{2+} to the measured current.

In this work, we use mathematical analysis to study the dynamics of the Ca^{2+} concentration in the outer segment of mouse rods and cones during a light response. To derive analytic results that provide quantitative insight, we use a spatially well-stirred phototransduction model that comprises the most relevant phototransduction steps [15]. In previous work, we analysed this model with the approximation that the free-Ca^{2+} concentration changes in proportion to the circulating current [15, 16]. Since however there is uncertainty about the degree of Ca^{2+} buffering in mouse rods and cones [17, 18, 19, 20], it is unclear how our previous results change if the Ca^{2+} dynamics becomes delayed with respect to the current, for example due to increased buffering. In this work we generalize our model by considering an explicit equation for the Ca^{2+} concentration, which allows for Ca^{2+} and current dynamics to differ. For dim-light stimulations, we derive analytic results that reveal the correlation between the electrical current and the change in the Ca^{2+} concentration. We use the model to predict the consequences of a change in Ca^{2+} concentration that is delayed with respect to the current, for example in experimental conditions with increased Ca^{2+} buffering. Finally, we examine how the photoresponse is affected by decreasing the extracellular Ca^{2+} concentration.

Materials and Methods

Phototransduction model

We use a spatially homogeneous signal transduction model for the outer segment (OS) similar to one previously described [16, 15] (see also [21, 19, 22, 20, 23]). In brief, light illumination generates activated visual pigment R^* with a rate that is proportional to the light intensity $\phi(t)$ times the collecting area κ. R^* deactivates with a rate μ_{rh} and generates the activated G-protein transducin T^* with a rate k_{act}. T^* deactivates with a rate μ_{tr} and generates activated phosphodiesterase (PDE) P^* with a rate k_{tr}. Because the deactivation of T^* is linked to the activation of PDE, we have $k_{tr} = \mu_{tr}$. P^* deactivates with a rate μ_{pde}, and hydrolyses the second messenger cyclic GMP (cGMP) with a

rate constant β_{sub}. The rate α by which the cGMP concentration c_{cg} is synthesized by guanylate cyclase depends on the free-Ca^{2+} concentration c_{ca}, $\alpha = \alpha_{max}\frac{r_\alpha c_{ca}^{n_\alpha}+K_\alpha^{n_\alpha}}{c_{ca}^{n_\alpha}+K_\alpha^{n_\alpha}}$, where $r_\alpha = \frac{\alpha_{min}}{\alpha_{max}} \leq 1$.

The total Ca^{2+} concentration in the OS comprising free and buffered Ca^{2+} changes due to influx via cGMP gated CNG channels and efflux via electrogenic NCKX exchangers [4, 21, 24, 25, 18, 6]. Ca^{2+} binds to and regulates the activity of several enzymes of the phototransduction cascade, for example, the activity of guanylate cyclase via the association with the Ca^{2+}- binding proteins GCAPs, or the rate of rhodopsin deactivation via binding to recoverin [26]. All these reactions contribute to Ca^{2+} buffering. The dynamics of free and buffered Ca^{2+} concentrations c_{ca,b_i} $(i = 1, \ldots N_b)$ are governed by the equations

$$\begin{aligned} F_A V_{os}\frac{d}{dt}\left(c_{ca} + \sum_{i=1}^{N_b} c_{ca,b_i}\right) &= \frac{I_{ch,ca}}{2} - I_{ex} \\ \frac{d}{dt}c_{ca,b_i} &= \mu_{ca,b_i}\left(\frac{(c_{ca,b_i,tot} - c_{ca,b_i})c_{ca}}{K_{ca,b_i}} - c_{ca,b_i}\right),\ i = 1, \ldots N_b\,, \end{aligned} \tag{1}$$

where $F_A = 9.65 \times 10^{-5}\frac{spA}{\mu M \mu m^3}$ is the Faraday constant, V_{os} is the outer segment volume, $I_{ch,ca}$ is the Ca^{2+}-current through CNG channels, I_{ex} is the exchanger current, $c_{ca,b_i,tot}$ are the total buffer concentrations, K_{ca,b_i} are dissociation constants, and μ_{ca,b_i} are dissociation rates. We further assume that Ca^{2+} feedback is fast and that the buffering reactions proceed quickly (more precisely, the time scales μ_{ca,b_i}^{-1} are small compared to the time scale of the current dynamics). In this case, the buffered concentrations $c_{ca,b_i}(t)$ can be approximated to be a function of the free Ca^{2+} concentration $c_{ca}(t)$, $c_{ca,b_i}(t) \approx c_{ca,b_i,tot}\frac{c_{ca}(t)}{c_{ca}(t)+K_{ca,b_i}}$ (quasi-steady-state approximation). With fast buffering we get from Eq. 1 for free Ca^{2+}

$$F_A V_{os}\left(1 + \sum_{i=1}^{N_b} B_{ca,b_i}\frac{(c_{ca,0} + K_{ca,b_i})^2}{(c_{ca} + K_{ca,b_i})^2}\right)\frac{d}{dt}c_{ca} = \frac{I_{ch,ca}}{2} - I_{ex}\,, \tag{2}$$

where $c_{ca,0}$ is the steady state concentration of free Ca^{2+} in darkness, and we defined the dark buffering constants $B_{ca,b_i} = \frac{c_{ca,b_i,tot}K_{ca,b_i}}{(c_{ca,0}+K_{ca,b_i})^2}$. The exchanger stoichiometry is such that the extrusion of a single Ca^{2+} ion leads to the influx of a single positive charge e^+ [4]. The exchanger current as a function of c_{ca} is $I_{ex} = I_{ex,sat}p_{ex}$, where $I_{ex,sat}$ is the saturating current at high c_{ca}, and $p_{ex} = \frac{c_{ca}}{c_{ca}+K_{ex}}$ determines the saturation level of the exchanger. The Ca^{2+} current $I_{ch,ca}$ through CNG channels is $I_{ch,ca} = I_{ch,ca,max}p_{ch}$, where $p_{ch} = \frac{c_{cg}^{n_{ch}}}{c_{cg}^{n_{ch}}+K_{ch}^{n_{ch}}}$ is the fraction of open channels, and K_{ch} is the $cGMP$ concentration where 50% of the CNG channels are open. The current $I_{ch,ca}$ corresponds to the fraction $f_{ch,ca}$ of the total CNG current I_{ch}.

Next we introduce the new variables $\tilde{P}^* = \beta_{sub}P^*$, $\tilde{T}^* = \frac{\beta_{sub}k_{tr}}{\mu_{pde}}T^*$, $\tilde{R}^* = \frac{\beta_{sub}k_{act}k_{tr}}{\mu_{pde}\mu_{tr}}R^*$. We define the modified light intensity $\tilde{\phi}(t) = \phi(t)\kappa\xi$, where $\xi = \frac{k_{act}\beta_{sub}k_{tr}}{\mu_{rh}\mu_{pde}\mu_{tr}} = \frac{k_{act}\beta_{sub}}{\mu_{rh}\mu_{pde}}$ is the gain (or amplification) of the PDE activation cascade. We use the measured steady state concentrations in darkness $c_{cg,0}$ and $c_{ca,0}$ to normalize variables and parameters: $\hat{c}_{cg} = \frac{c_{cg}}{c_{cg,0}}$, $\hat{c}_{ca} = \frac{c_{ca}}{c_{ca,0}}$, $\hat{K}_{ch} = \frac{K_{ch}}{c_{cg,0}}$, $\hat{K}_{ex} = \frac{K_{ex}}{c_{ca,0}}$, $\hat{K}_\alpha = \frac{K_\alpha}{c_{ca,0}}$, and $\hat{K}_{ca,b_i} = \frac{K_{ca,b_i}}{c_{ca,0}}$. With the steady state conditions $I_{ch,ca,0} = 2I_{ex,0}$ and $\alpha_0 = \beta_d c_{cg,0}$, where β_d is the basal cGMP hydrolysis rate in darkness, we obtain the system of

equations

$$
\begin{aligned}
\frac{d}{dt}\tilde{R}^* &= \mu_{rh}(\tilde{\phi}(t) - \tilde{R}^*) \\
\frac{d}{dt}\tilde{T}^* &= \mu_{tr}(\tilde{R}^* - \tilde{T}^*) \\
\frac{d}{dt}\tilde{P}^* &= \mu_{pde}(\tilde{T}^* - \tilde{P}^*) \\
\frac{d}{dt}\hat{c}_{cg} &= \beta_d\hat{\alpha} - (\beta_d + \tilde{P}^*)\hat{c}_{cg} \\
\frac{d}{dt}\hat{c}_{ca} &= \frac{1 + B_{ca}}{1 + \sum_{i=1}^{N_b} B_{ca,b_i}\frac{(1+\hat{K}_{ca,b_i})^2}{(\hat{c}_{ca}+\hat{K}_{ca,b_i})^2}}\mu_{ca}\left(\hat{p}_{ch} - \hat{p}_{ex}\right)
\end{aligned}
\tag{3}
$$

where we introduced

$$
\begin{aligned}
B_{ca} &= \sum_{i=1}^{N_b} B_{ca,b_i} \\
\mu_{ca} &= \frac{1}{(1+B_{ca})F_A V_{os}}\frac{I_{ex,0}}{c_{ca,0}} = \frac{1}{(1+B_{ca})F_A V_{os}}\frac{f_{ch,ca}}{f_{ch,ca}+2}\frac{I_0}{c_{ca,0}} \\
\hat{\alpha} &= \frac{\alpha}{\alpha_0} = \frac{1+\hat{K}_\alpha^{n_\alpha}}{r_\alpha + \hat{K}_\alpha^{n_\alpha}}\frac{r_\alpha \hat{c}_{ca}^{n_\alpha} + \hat{K}_\alpha^{n_\alpha}}{\hat{c}_{ca}^{n_\alpha} + \hat{K}_\alpha^{n_\alpha}} \\
\hat{p}_{ch} &= \frac{I_{ch,ca}}{I_{ch,ca,0}} = \frac{1+\hat{K}_{ch}^{n_{ch}}}{\hat{c}_{cg}^{n_{ch}} + \hat{K}_{ch}^{n_{ch}}}\hat{c}_{cg}^{n_{ch}} \\
\hat{p}_{ex} &= \frac{I_{ex}}{I_{ex,0}} = \frac{1+\hat{K}_{ex}}{\hat{c}_{ca} + \hat{K}_{ex}}\hat{c}_{ca}\,.
\end{aligned}
\tag{4}
$$

The steady state currents in darkness are $I_{ch,0} = \frac{2}{f_{ch,ca}+2}I_0$, $I_{ex,0} = \frac{f_{ch,ca}}{f_{ch,ca}+2}I_0$, and $I_0 = I_{ch,0} + I_{ex,0}$ is the overall dark current. The current $I = I_{ch} + I_{ex}$ normalized by I_0 is

$$
\hat{I} = \hat{I}_{ch} + \hat{I}_{ex} = \frac{2}{f_{ch,ca}+2}\hat{p}_{ch} + \frac{f_{ch,ca}}{f_{ch,ca}+2}\hat{p}_{ex}\,. \tag{5}
$$

We further introduce the current change $\hat{i} = 1 - \hat{I}$, which is zero in darkness.

For large μ_{ca}, the equation for $\hat{c}_{ca}$ in Eq. 3 can be replaced with the approximation $\hat{p}_{ch} \approx \hat{p}_{ex}$. The time dependent current is now given by the steady state expression $\hat{I} \approx \hat{p}_{ch} \approx \hat{p}_{ex}$. Moreover, since for $\hat{K}_{ex} \gg 1$ we have $\hat{p}_{ex} \approx \hat{c}_{ca}$, we obtain $\hat{c}_{ca} \approx \hat{I}$. Thus, for large μ_{ca} we obtain that the Ca^{2+} concentration changes in proportion to the current, and we recover our results from [15, 16]. We now generalize our previous results by studying how electrical current and Ca^{2+} dynamics are affected if the rate μ_{ca} decreases, for example, due to increased buffering or treatment with the calcium buffer BAPTA.

Analytic results for dim-light

The equations for PDE activation in Eq. 3 are linear and can be solved analytically,

$$
\tilde{P}^*(t) = \int_0^t \tilde{\phi}(s)G_p(t-s)ds \tag{6}
$$

with the Green's function

$$
G_p(t) = \frac{\mu_{rh}\mu_{tr}\mu_{pde}}{(\mu_{rh}-\mu_{tr})(\mu_{rh}-\mu_{pde})}e^{-\mu_{rh}t} + (\mu_{rh} \leftrightarrow \mu_{tr}) + (\mu_{rh} \leftrightarrow \mu_{pde})\,, \tag{7}
$$

where the double-headed arrows signify that the second and third terms in the equation are identical to the first term with the exchange μ_{tr} and μ_{rh} in the second term, and μ_{pde} and μ_{rh} in the third term. The equations for $\hat{c}_{cg}$ and $\hat{c}_{ca}$ cannot be solved analytically for all conditions of light stimulation $\phi(t)$. However, analytic results can be derived for dim-light intensities by linearizing Eq. 3. For the analysis we introduce $y = -\ln \hat{c}_{cg}$ and $z = -\ln \hat{c}_{ca}$, which are both zero in darkness. With $y \ll 1$, $z \ll 1$, $\hat{p}_{ch} \approx 1 - \frac{\hat{K}_{ch}^{n_{ch}}}{1+\hat{K}_{ch}^{n_{ch}}} n_{ch} y$, $\hat{p}_{ex} \approx 1 - \frac{\hat{K}_{ex}}{1+\hat{K}_{ex}} z$, we obtain from Eq. 3 the first order equations

$$\begin{aligned} \frac{d}{dt} y &= \tilde{P}^* - \beta_d (y + \hat{\alpha}_0' z) \\ \frac{d}{dt} z &= \beta_d r \left(\tilde{n}_{ch} y - z \right) , \end{aligned} \tag{8}$$

where

$$\begin{aligned} \hat{\alpha}_0' &= \frac{d}{dz} \hat{\alpha}(z) \Big|_{z=0} = -\frac{d}{d\hat{c}_{ca}} \hat{\alpha}(\hat{c}_{ca}) \Big|_{\hat{c}_{ca}=1} = \frac{n_\alpha \hat{K}_\alpha^{n_\alpha} (1 - r_\alpha)}{(1 + \hat{K}_\alpha^{n_\alpha})(\hat{K}_\alpha^{n_\alpha} + r_\alpha)} \\ \tilde{n}_{ch} &= \frac{1 + \hat{K}_{ex}}{\hat{K}_{ex}} \frac{\hat{K}_{ch}^{n_{ch}}}{1 + \hat{K}_{ch}^{n_{ch}}} n_{ch} \\ r &= \frac{\mu_{ca}}{\beta_d} \frac{\hat{K}_{ex}}{1 + \hat{K}_{ex}} . \end{aligned} \tag{9}$$

For GCAPs$^{-/-}$ mutants where the cyclase is no longer Ca^{2+} dependent we have $\hat{\alpha}_0' = 0$. The solutions of Eq. 8 with $\tilde{P}^* = \int_0^t \tilde{\phi}(s) G_p(t-s) ds$ are

$$y(t) = \sum_{i=1}^{2} \zeta_{y,i} \int_0^t \tilde{\phi}(s) G_i(t-s) ds , \quad z(t) = \sum_{i=1}^{2} \zeta_{z,i} \int_0^t \tilde{\phi}(s) G_i(t-s) ds , \tag{10}$$

where $\zeta_{y,1} = \frac{r-\lambda_1}{\lambda_2-\lambda_1}$, $\zeta_{y,2} = \frac{r-\lambda_2}{\lambda_1-\lambda_2}$, $\zeta_{z,1} = \frac{\tilde{n}_{ch} r}{\lambda_2-\lambda_1}$ and $\zeta_{z,2} = \frac{\tilde{n}_{ch} r}{\lambda_1-\lambda_2}$. The parameters $\lambda_1 = \frac{1+r}{2} - \frac{\sqrt{(r-1)^2 - 4\tilde{n}_{ch}\hat{\alpha}_0' r}}{2}$ and $\lambda_2 = \frac{1+r}{2} + \frac{\sqrt{(r-1)^2 - 4\tilde{n}_{ch}\hat{\alpha}_0' r}}{2}$ are the eigenvalues of the matrix $\begin{pmatrix} 1 & \hat{\alpha}_0' \\ -\tilde{n}_{ch} r & r \end{pmatrix}$. The Green's functions are $(i = 1, 2)$

$$\begin{aligned} G_i(t) &= -\frac{\mu_{rh}\mu_{tr}\mu_{pde} e^{-\mu_{rh} t}}{(\mu_{rh} - \mu_{tr})(\mu_{rh} - \mu_{pde})(\mu_{rh} - \beta_d \lambda_i)} + (\mu_{rh} \leftrightarrow \mu_{tr}) + (\mu_{rh} \leftrightarrow \mu_{pde}) + (\mu_{rh} \leftrightarrow \beta_d \lambda_i) \\ &= G_{rh}(t) + G_{tr}(t) + G_{pde}(t) + G_{\beta_i}(t) , \end{aligned} \tag{11}$$

where the double-headed arrows have the same significance as previously. For a light step at $t = 0$ with duration Δt and intensity ϕ that generates $R_0^* = \kappa \phi \Delta t$ isomerisations, we get $y(t) = R_0^* \xi g_y(t)$, $z(t) = R_0^* \xi g_z(t)$, where

$$g_y(t) = \sum_{i=1}^{2} \zeta_{y,i} \frac{1}{\Delta t} \int_0^{\min(t,\Delta t)} G_i(t-s) ds , \quad g_z(t) = \sum_{i=1}^{2} \zeta_{z,i} \frac{1}{\Delta t} \int_0^{\min(t,\Delta t)} G_i(t-s) ds . \tag{12}$$

The current is $\hat{i} \approx \frac{2}{f_{ch,ca}+2} \frac{\hat{K}_{ch}^{n_{ch}}}{1+\hat{K}_{ch}^{n_{ch}}} n_{ch} y + \frac{f_{ch,ca}}{f_{ch,ca}+2} \frac{\hat{K}_{ex}}{1+\hat{K}_{ex}} z = R_0^* \hat{i}_{spr}$, where the response to a single isomerisation is

$$\hat{i}_{spr} = \xi n_{ch} \frac{\hat{K}_{ch}^{n_{ch}}}{1 + \hat{K}_{ch}^{n_{ch}}} \frac{2}{f_{ch,ca} + 2} \left(g_y + \frac{f_{ch,ca}}{2\tilde{n}_{ch}} g_z \right) . \tag{13}$$

With Eq. 11 we obtain the decomposition

$$\hat{i}_{spr} = \hat{i}_{spr,rh} + \hat{i}_{spr,tr} + \hat{i}_{spr,pde} + \hat{i}_{spr,\beta_1} + \hat{i}_{spr,\beta_2} = \hat{i}_{spr,rh} + \hat{i}_{spr,tr} + \hat{i}_{spr,pde} + \hat{i}_{spr,\beta}\,. \tag{14}$$

For short flashes, $\hat{i}_{spr}$ corresponds to the single-photon response (SPR). With $\frac{1}{\Delta t}\int_0^{\min(t,\Delta t)} G_i(t-s) \approx G_i(t)$ we find $\hat{i}_{spr,rh} \sim e^{-\mu_{rh}t}$, $\hat{i}_{spr,tr} \sim e^{-\mu_{tr}t}$, $\hat{i}_{spr,pde} \sim e^{-\mu_{pde}t}$, $\hat{i}_{spr,\beta_1} \sim e^{-\beta_d\lambda_1 t}$, and $\hat{i}_{spr,\beta_2} \sim e^{-\beta_d\lambda_2 t}$.

In the limit of fast Ca^{2+} dynamics, $\mu_{ca} \to \infty$ ($r \to \infty$), we have $\lambda_1 \to 1 + \tilde{n}_{ch}\hat{\alpha}'_0$, $\lambda_2 \to \infty$ and $\hat{i}_{spr,\beta} \sim e^{-\beta_d\lambda_1 t}$. In this limit we also have $\hat{p}_{ch} \approx \hat{p}_{ex}$ and $\hat{I} \approx \hat{p}_{ex} \approx \hat{c}_{ca}$, showing that the Ca^{2+} concentration changes proportional to the current. In the opposite limit of slow Ca^{2+} dynamics, $\mu_{ca} \to 0$ ($r \to 0$), we have $\lambda_1 \to 1$, $\lambda_2 \to 0$, $\zeta_{y,2} \to 0$, $\zeta_{z,2} \to 0$, such that $\hat{i}_{spr,\beta} \sim e^{-\beta_d t}$. This is also the result for the GCAPs$^{-/-}$ case with $\hat{\alpha}'_0 = 0$.

Damped oscillations

For $(r-1)^2 - 4\tilde{n}_{ch}\hat{\alpha}'_0 r < 0$, the eigenvalues λ_i are complex conjugate, and $\hat{i}_{spr,\beta} = \hat{i}_{spr,\beta_1} + \hat{i}_{spr,\beta_2}$ describes a damped oscillation. Such oscillations arise for $r_1 < r < r_2$, with the bifurcation points $r_1 = 1+2\tilde{n}_{ch}\hat{\alpha}'_0\left(1 - \sqrt{1+\frac{1}{\tilde{n}_{ch}\hat{\alpha}'_0}}\right)$ and $r_2 = 1+2\tilde{n}_{ch}\hat{\alpha}'_0\left(1 + \sqrt{1+\frac{1}{\tilde{n}_{ch}\hat{\alpha}'_0}}\right)$. By writing $\lambda_1 = \lambda_{re} - i\lambda_{im}$ and $\lambda_2 = \lambda_{re} + i\lambda_{im}$, with $\lambda_{re} = \dfrac{1+r}{2}$ and $\lambda_{im} = \frac{\sqrt{-(r-r_1)(r-r_2)}}{2}$, we get for a short flash

$$\hat{i}_{spr,\beta} = \xi n_{ch}\frac{\hat{K}_{ch}^{n_{ch}}}{1+\hat{K}_{ch}^{n_{ch}}}\frac{2}{f_{ch,ca}+2}\left(a_y\cos(\omega t+\varphi_y) + \frac{f_{ch,ca}}{2\tilde{n}_{ch}}a_z\cos(\omega t+\varphi_z)\right)e^{-\mu_{damp}t}\,, \tag{15}$$

with frequency $\omega = \beta_d\lambda_{im} = \beta_d\frac{\sqrt{-(r-r_1)(r-r_2)}}{2}$ and damping rate $\mu_{damp} = \beta_d\lambda_{re} = \beta_d\frac{1+r}{2}$. The oscillation amplitudes a_y and a_z, and the phases φ_y and φ_z can be computed with Eq. 11.

Steady state solution with a constant background light

With a constant light intensity ϕ we have $\hat{p}_{ch} = \hat{p}_{ex}$ and $\hat{I} = \hat{p}_{ch} = \hat{p}_{ex}$. The steady state solutions of Eq. 8 are $z = \tilde{n}_{ch}y$ and $y = \frac{\phi\kappa\xi}{\beta_d(1+\tilde{n}_{ch}\hat{\alpha}'_0)}$. The current is $\hat{i} = 1 - \hat{I} \approx \frac{\hat{K}_{ch}^{n_{ch}}}{1+\hat{K}_{ch}^{n_{ch}}}\frac{\phi\kappa\xi n_{ch}}{\beta_d(1+\tilde{n}_{ch}\hat{\alpha}'_0)} = \frac{\hat{K}_{ex}}{1+\hat{K}_{ex}}z$.

Impact of changing the extracellular Ca^{2+} concentration

To investigate how the light response changes when the extracellular Ca^{2+} concentration is altered, we assume that the previous analysis corresponds to a situation with extracellular concentration $\hat{c}_{ca,ex,0}$. We now compute the light response for the case that this extracellular concentration is changed by the factor $r_{ca,ex}$ to the new value $r_{ca,ex}\hat{c}_{ca,ex,0}$. We assume that the CNG current carried by Ca^{2+} changes in proportion to the extracellular Ca^{2+} concentration, $\hat{I}_{ch,ca} = r_{ca,ex}\hat{I}_{ch,ca,0}\hat{p}_{ch} = r_{ca,ex}f_{ch,ca}\frac{2}{f_{ch,ca}+2}\hat{p}_{ch}$, and that the CNG current that is not carried by Ca^{2+} remains unaffected, $\hat{I}_{ch,\overline{ca}} = (1-f_{ch,ca})\frac{2}{f_{ch,ca}+2}\hat{p}_{ch}$. The overall CNG current with modified extracellular Ca^{2+} thus is $\hat{I}_{ch} = \hat{I}_{ch,ca} + \hat{I}_{ch,\overline{ca}} = \frac{\hat{I}_{ch,ca}}{f'_{ch,ca}}$, where $f'_{ch,ca} = f_{ch,ca}\frac{r_{ca,ex}}{1+(r_{ca,ex}-1)f_{ch,ca}}$ is the new fraction of the channel current carried by Ca^{2+}. The new dark steady-state values $\hat{c}_{ca,d}$ and $\hat{c}_{cg,d} = \hat{\alpha}(\hat{c}_{ca,d})$ are obtained numerically by solving the equation $\frac{\hat{I}_{ch,ca}}{2} - \hat{I}_{ex} = 0$, which is $r_{ca,ex}\frac{1+\hat{K}_{ch}^{n_{ch}}}{\hat{\alpha}(\hat{c}_{ca,d})^{n_{ch}}+\hat{K}_{ch}^{n_{ch}}}\hat{\alpha}(\hat{c}_{ca,d})^{n_{ch}} - \frac{1+\hat{K}_{ex}}{\hat{c}_{ca,d}+\hat{K}_{ex}}\hat{c}_{ca,d} = 0$. The new dark current is $\hat{I}_d = \frac{f'_{ch,ca}+2}{f'_{ch,ca}}\hat{I}_{ex,0}\hat{p}_{ex,d} = \frac{f'_{ch,ca}+2}{f'_{ch,ca}}\frac{f_{ch,ca}}{f_{ch,ca}+2}\frac{1+\hat{K}_{ex}}{\hat{c}_{ca,d}+\hat{K}_{ex}}\hat{c}_{ca,d}$. Finally, we use the new values $f'_{ch,ca}$, $c'_{ca,0} = \hat{c}_{ca,d}c_{ca,0}$, $c'_{cg,0} = \hat{c}_{cg,d}c_{cg,0}$ and $I'_0 = \hat{I}_d I_0$ together with our previous analysis to study the light-response with modified extracellular Ca^{2+} concentration.

Results

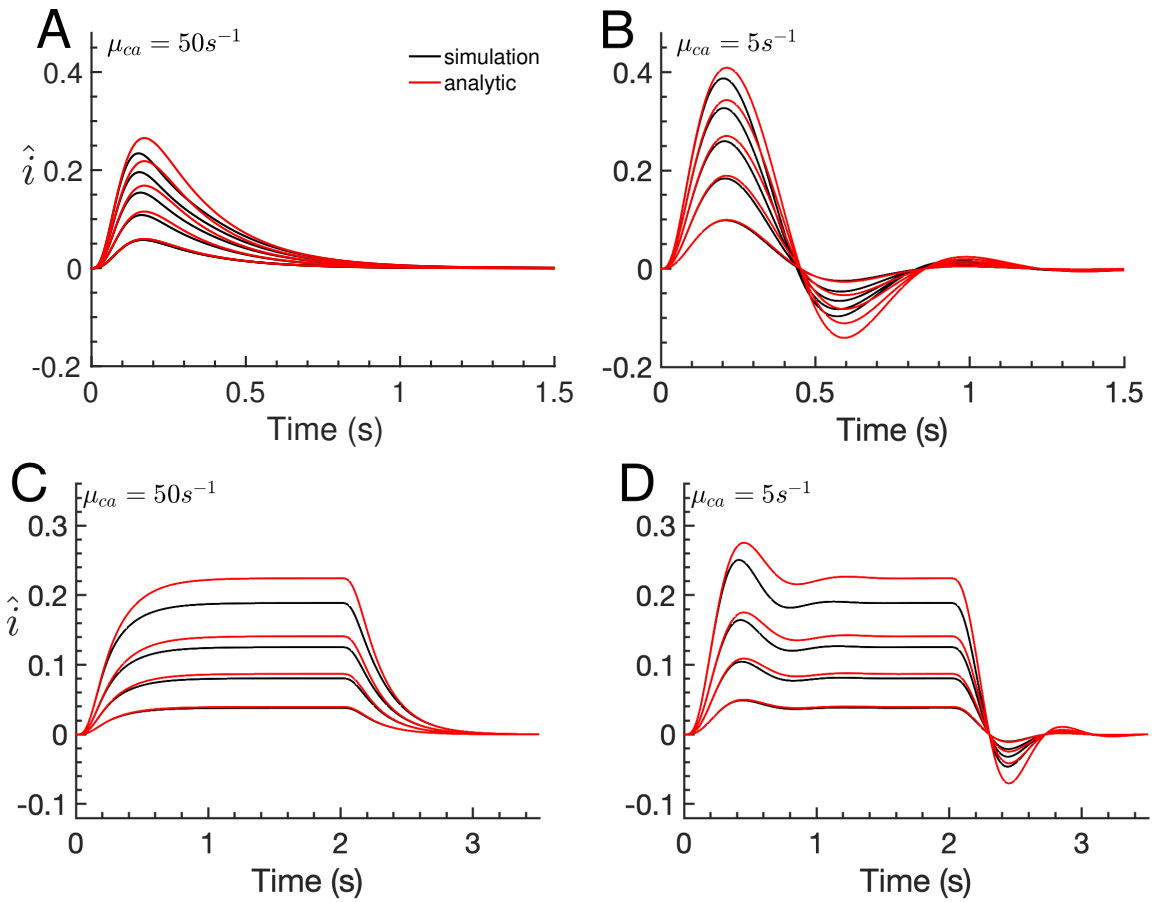

Figure 1: **Simulations and analytic results for a rod.** Comparison of simulations with analytic results for the current $\hat{i}$ with fast and slow Ca^{2+} dynamics for flashes with duration $\Delta t = 0.01s$ (A-B) and steps with duration $\Delta t = 2s$ (C-D) The number of isomerisations $R_0^* = \kappa\phi\Delta t$ are: $R_0^* = 1, 2, 3, 4, 5$ (A-B) and $R_0^* = 4, 9, 15, 25$ (C-D). Simulations are computed with Eq. 3 and a single buffering species. Analytic results are obtained with Eq. 13. The value of μ_{ca} is indicated in each panel. The remaining parameters are as in Table 1.

In the limit of large μ_{ca} and with $\hat{K}_{ex} \gg 1$ (see Table 1), Eq. 3 reduces to a model where the free-Ca^{2+} concentration changes in proportion to the current, $\hat{c}_{ca} \approx \hat{I}$. We previously analysed and calibrated such a model using dim-flash recordings for mouse WT and GCAPs$^{-/-}$ rods and cones [15, 16]. We now use these parameters to study how the photoresponse changes as the value of μ_{ca} decreases, for example, due to increased buffering. Buffering affects the photoresponse in Eq. 3 via the rate μ_{ca} that depends on the overall buffering constant B_{ca} (see Eq. 4), and via the term $(1 + B_{ca})/(1 + \sum_{i=1}^{N_b} B_{ca,b_i} \frac{(1+\hat{K}_{ca,b_i})^2}{(\hat{c}_{ca}+\hat{K}_{ca,b_i})^2})$, which is normalized to one in darkness and depends on the properties of the individual buffer species. However, in first approximation the latter term does not affect the photoresponse (see Eq. 8), and more generally, simulations show that its impact on the dim-light response is small (not shown). Thus, in the following we will study the Ca^{2+}-dynamics for

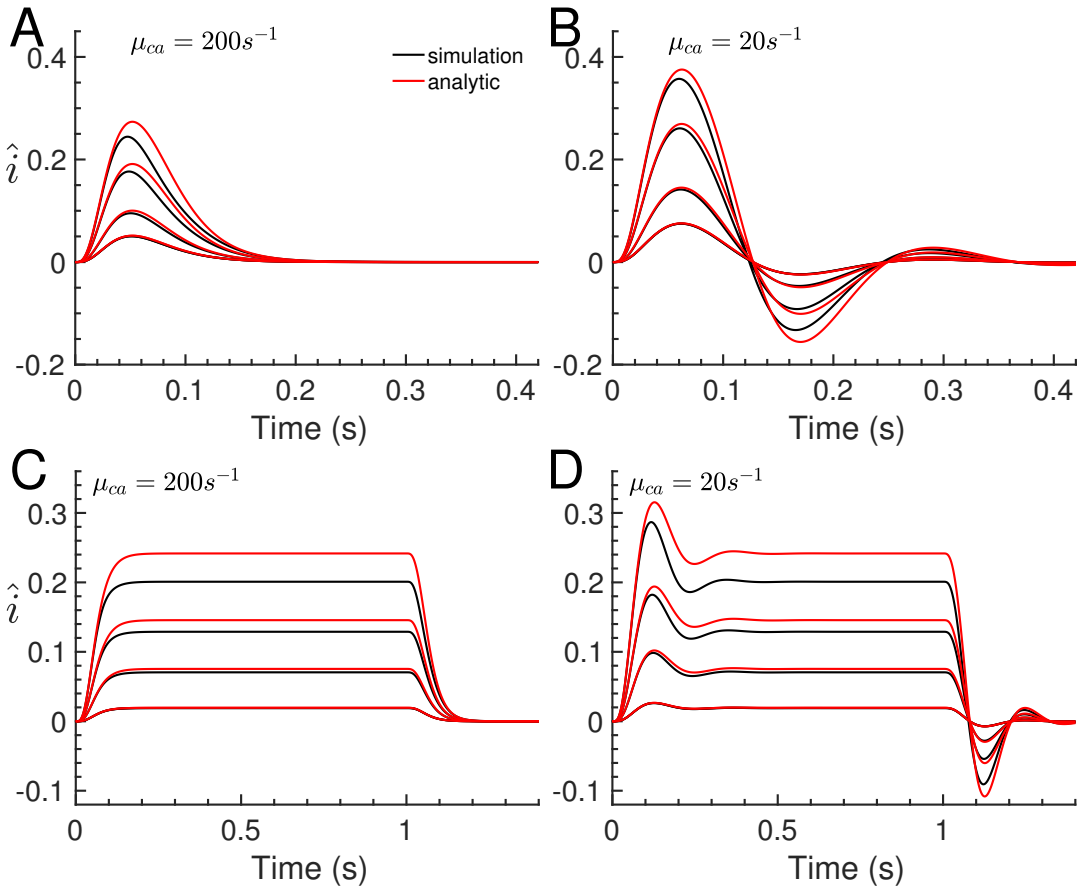

Figure 2: **Simulations and analytic results for a cone.** Comparison of simulations with analytic results for the current $\hat{i}$ with fast and slow Ca^{2+} dynamics for flashes with duration $\Delta t = 0.005s$ (A-B) and step responses with duration $\Delta t = 1s$ (C-D). The number of isomerisations $R_0^* = \kappa\phi\Delta t$ are: $R_0^* = 130, 260, 520, 780$ (A-B) and $R_0^* = 650, 2600, 5200, 9100$ (C-D). Simulations are computed with Eq. 3 and a single buffering species. Analytic results are obtained with Eq. 13. The value of μ_{ca} is indicated in each panel. The remaining parameters are as in Table 1.

dim-light responses by focusing on μ_{ca}.

Validity range of the analytic results

We first check the validity range of our analysis by comparing simulations and analytic results for the normalized current $\hat{i}$ for rod and cone flash and step responses, and for two scenarios with fast and slow μ_{ca} ($\mu_{ca} = 50s^{-1}$ and $\mu_{ca} = 5s^{-1}$ for rod; $\mu_{ca} = 200s^{-1}$ and $\mu_{ca} = 20s^{-1}$ for cone). Simulations are computed with Eq. 3, the analytic result is $\hat{i} = R_0^*\hat{i}_{spr}$, where $R_0^* = \phi\kappa\Delta t$ are the number isomerisations produced by the light intensity ϕ during the stimulation time Δt, and $\hat{i}_{spr}$ is the unitary response defined in Eq. 13. Because recoverin is the most abundant calcium buffer in the outer segment [4, 26], we performed simulations with only a single buffering species with dissociation constant $K_{ca,b} = 3\mu M$ corresponding to the reaction between Ca^{2+} and recoverin [27]. Except for μ_{ca}, all other parameters are as specified in Table 1. We modify the value of μ_{ca} by changing B_{ca} (see Eq. 4). For example, with $B_{ca} = 50$ [24] we have $\mu_{ca} \approx 184s^{-1}$ for a cone, and $\mu_{ca} \approx 32s^{-1}$ for

a rod.

For dim-light, we find that the rod and cone simulations precisely agree with the analytic results for flash responses with fast and slow Ca^{2+} dynamics (Fig. 1A-B and Fig. 2A-B, black vs red curves), as well as step responses with fast and slow Ca^{2+} dynamics (Fig. 1C-D and Fig. 2C-D, black vs red curves). As the light intensity increases, the analytic results overestimate the current response because the linear approximation underestimates the non-linear increase in negative Ca^{2+} feedback to the cyclase. For large μ_{ca} we observe monophasic responses (Fig. 1A,C and Fig. 2A,C), whereas for small μ_{ca} we observe the emergence of damped oscillations (Fig. 1B,D and Fig. 2B,D), as predicted by Eq. 15. In summary, we conclude that our analytic formulas can be faithfully applied to study the dim-light photoreceptor response.

Unitary flash and step response

Because dim-light responses are proportional to the number of isomerisations R_0^*, it is sufficient to focus on the unitary response $\hat{i}_{spr}$. For flashes with short duration Δt, $\hat{i}_{spr}$ corresponds to the classical single-photon response (SPR). For steps with longer Δt, $\hat{i}_{spr}$ corresponds to a response function.

The SPR time-to-peak and amplitude decrease as μ_{ca} increases, because a faster Ca^{2+} dynamics leads to quicker cyclase activation and more negative feedback (Fig. 3A,B, solid lines). In the opposite limit $\mu_{ca} \to 0$, we have that the Ca^{2+} concentration remains constant and there is no cyclase feedback. This is similar to GCAPs$^{-/-}$ photoreceptors where the Ca^{2+} feedback to the cyclase is absent ($\hat{\alpha}_0' = 0$). However, whereas in GCAPs$^{-/-}$ photoreceptors the Ca^{2+} concentration can still vary, this is not the case in the limit $\mu_{ca} \to 0$. We find that affecting the Ca^{2+} dynamics has only little impact on the dim-light response in GCAPs$^{-/-}$ photoreceptors (Fig. 3A,B, dashed lines). The small current modulation as a function of μ_{ca} is due to the exchanger current, which depends on the Ca^{2+} concentration. Hence, we conclude that changing the Ca^{2+} dynamics affects the dim-light response predominantly via the cyclase feedback.

Before we continue, we first add some definitions to better characterise flash and step responses. For flash responses, we define the rising phase as the response up to the time-to-peak, and the recovery phase as the remainder of the response (Fig. 3A-B). For step responses, we define the initial phase up to the time where the response approximately reaches the plateau value, the intermediate plateau phase up to the time where the light is switched off, and the recovery phase for the remainder of the response (Fig. 3C-D)

For step responses with sufficiently long stimulation time Δt, the initial and recovery phases depend on μ_{ca}, whereas the plateau phase is independent of μ_{ca} and is determined by steady-state properties (Fig. 3C-D, solid lines). The GCAPs$^{-/-}$ plateau is larger compared to WT by a factor of $1 + \tilde{n}_{ch}\hat{\alpha}_0'$ (see the steady state analysis after Eq. 15). From the values in Table 1, we compute $\tilde{n}_{ch} \approx 2.92$, $\hat{\alpha}_0' \approx 1.37$ and $1 + \tilde{n}_{ch}\hat{\alpha}_0' \approx 5$. Thus, whereas the plateau values of WT and GCAPs$^{-/-}$ step responses are independent of μ_{ca} and differ by a factor of around 5 (Fig. 3C-D), the WT and GCAPs$^{-/-}$ SPR amplitudes depend on μ_{ca} and differ maximally by a factor of around 2-3, achieved for fast Ca^{2+} dynamics (Fig. 3A-B).

Waveform of a dim-light response

To study how the rate constant μ_{ca} of the change in Ca^{2+} affects the shape of a short flash response, we introduce the normalized current waveform by normalizing $\hat{i}$ from Fig. 3A with the peak value of the flash response amplitude (Fig. 4A). For steps, we define the waveform by normalizing $\hat{i}$ from Fig. 3C with the plateau value (Fig. 4B). We use $1 - \hat{c}_{ca}$ to characterize the Ca^{2+} waveform in order to study the delay between the current and the Ca^{2+} concentration (Fig. 4C-D).

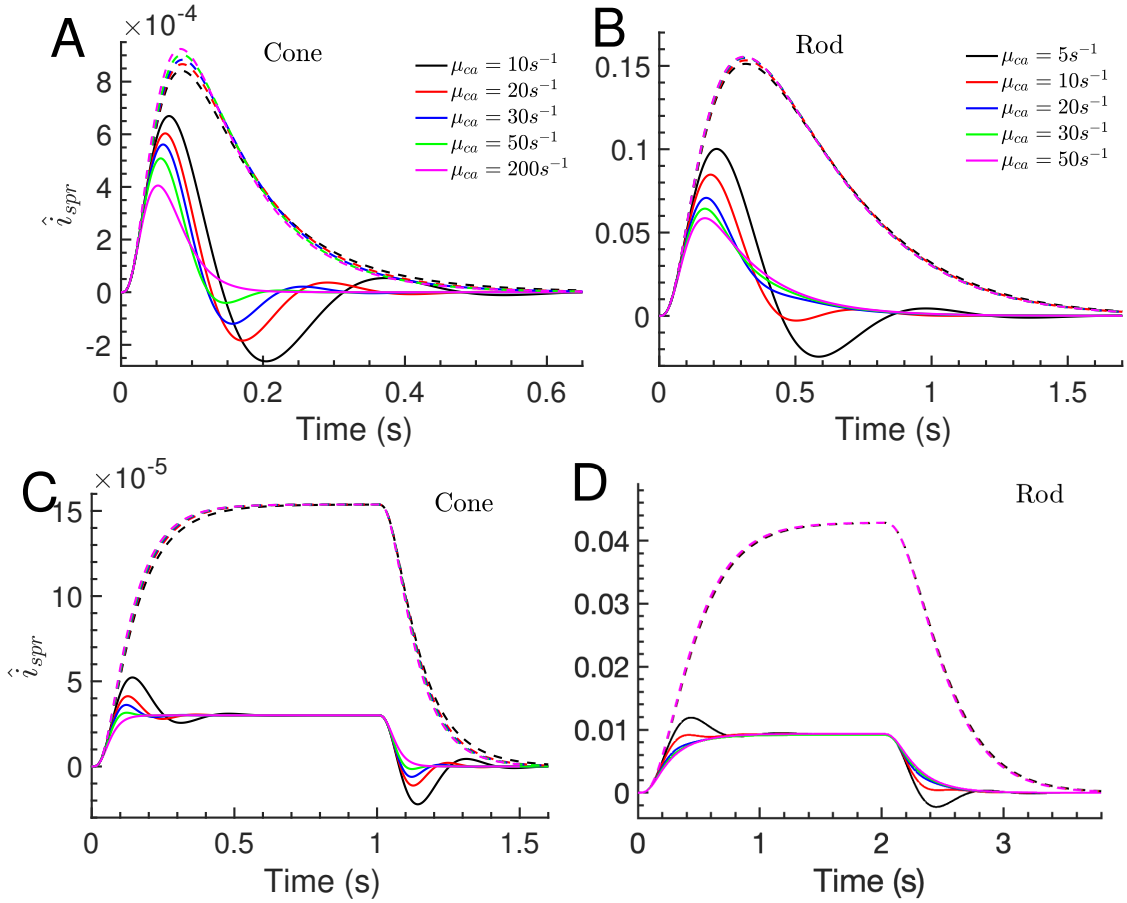

Figure 3: **Unitary flash and step response $\hat{i}_{spr}$.** Unitary flash (A-B) and step responses (C-D) for WT (solid lines) and GCAPs$^{-/-}$ (dashed lines) rod and cone for various μ_{ca}. Steps have stimulation time $\Delta t = 1s$ (cone) and $\Delta t = 2s$ (rod). Curves are computed with Eq. 13. For GCAPs$^{-/-}$ photoreceptors we have $\hat{\alpha}'_0 = 0$. For flashes, the unitary response corresponds to the single-photon response (SPR).

The current waveform is monophasic for large μ_{ca} (Fig. 4A-B, magenta curves). In this limit, the Ca^{2+} dynamics are determined by the current, and the waveforms of both the current and Ca^{2+} are similar (Fig. 4C-D, green curves). Indeed, for large μ_{ca} we have $\hat{p}_{ch} \approx \hat{p}_{ex}$ (see Eq. 3), $\hat{I} \approx \hat{p}_{ex}$, and $\hat{p}_{ex} \approx \hat{c}_{ca}$ (valid for $\hat{K}_{ex} \gg 1$) we get $\hat{I} \approx \hat{c}_{ca}$ and $\hat{i} \approx 1 - \hat{c}_{ca}$. As μ_{ca} decreases, damped oscillations emerge (Fig. 4A-B) because the Ca^{2+} dynamics becomes delayed with respect to the current (Fig. 4C-D, red and black curves). In limit $\mu_{ca} \to 0$ the current response becomes again monophasic (see the GCAPs$^{-/-}$ curves in Fig. 3) because the Ca^{2+} concentration remains constant and there is no cyclase modulation (not shown).

Although the rising and recovery phases of the the dim-flash waveform are different (Fig. 4A), the initial and recovery phases of dim-step responses are symmetric (Fig. 4B). Because Eq. 8 is linear, for sufficiently large Δt we find that both rising and recovery phases are related by $\hat{i}_{step}(\Delta t + t) = \hat{i}_{ss} - \hat{i}_{step}(t)$ $(t < \Delta t)$, where $\hat{i}_{ss}$ is the plateau value.

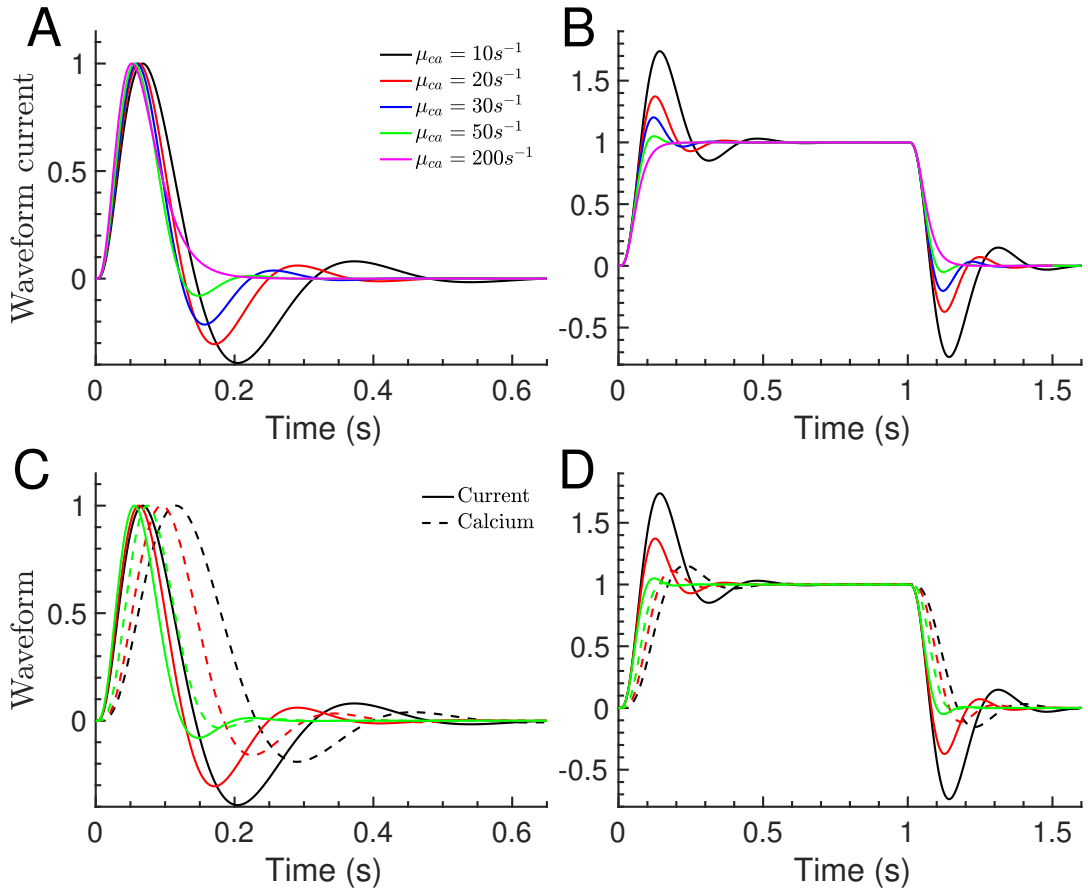

Figure 4: **Waveforms of dim-light cone responses**. (A) The flash responses from Fig. 3A are normalized to unit amplitude. (B) The step responses from Fig. 3C are normalized with the plateau value. (C-D) Ca^{2+} waveforms are computed with $1 - \hat{c}_a$ and compared to the current waveforms from (A-B) for $\mu_{ca} = 10, 20, 50s^{-1}$ (same colors as in A-B).

Decomposition of the SPR waveform

We next used our analytic result in Eq. 14 to dissect the dim-flash waveform in order to display the contributions coming from the various biophysical processes. Such a decomposition cannot be obtained from simulations, for which the absence of an analytic expression precludes identification of the components contributing to the response. We find that the recovery in a rod with fast Ca^{2+} dynamics is limited by PDE decay (Fig. 5A)). For a GCAPs$^{-/-}$ cone the recovery is limited by the basal turnover rate β_d, $\hat{i}_{spr,\beta} \sim e^{-\beta_d t}$ (Fig. 5B; the value of μ_{ca} has only little impact, see Fig. 3A). For these two cases, biophysical parameters can be reliably extracted by fitting the late recovery phase with a single exponential.

In general, however, the recovery of a flash responses is not limited by a single biophysical process. For example, for rod resp. cone with slow Ca^{2+} dynamics $\mu_{ca} = 5s^{-1}$ resp. $\mu_{ca} = 20s^{-1}$, the recovery is determined by the damped oscillation originating from the Ca^{2+} dependent interaction between cGMP and cyclase (Fig. 5C-D). In these cases, fitting the recovery phase with a single exponential does is not meaningful.

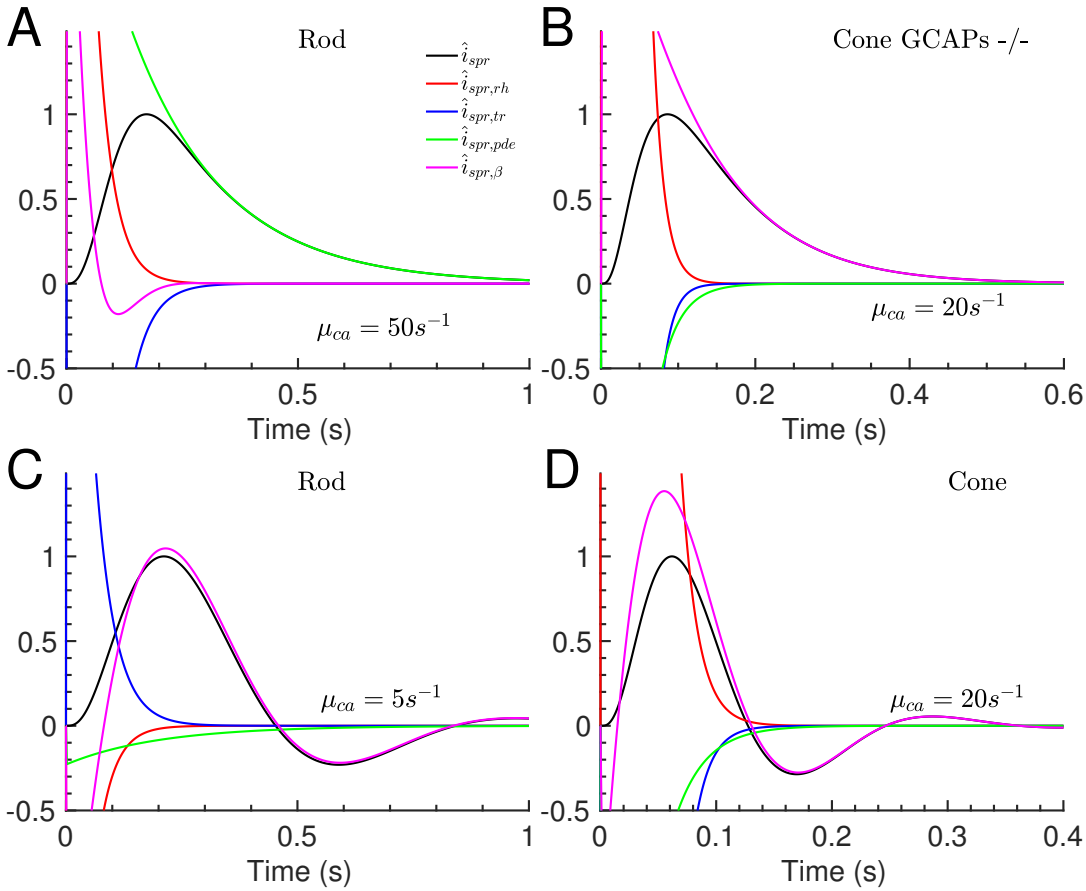

Figure 5: **Decomposition of the SPR waveform**. (A) Decomposition for a WT rod with $\mu_{ca} = 50s^{-1}$, (B) GCAPs$^{-/-}$ cone with $\mu_{ca} = 20s^{-1}$, (C) WT rod with $\mu_{ca} = 5s^{-1}$, (D) WT cone with $\mu_{ca} = 20s^{-1}$. Curves are computed with Eq. 14.

Damped Ca^{2+} oscillations

If the ratio $r = \frac{\mu_{ca}}{\beta_d}\frac{\hat{K}_{ex}}{1+\hat{K}_{ex}}$ (Eq. 4) is within the range $r_1 < r < r_2$, where r_1 and r_2 depend on $\tilde{n}_{ch}\hat{\alpha}'_0$ (see analysis before Eq. 15), the current component $\hat{i}_{spr,\beta}$ in Eq. 14 describes a damped oscillation with damping rate $\mu_{damp} = \beta_d\frac{1+r}{2} \approx \frac{\beta_d+\mu_{ca}}{2}$ and frequency $\omega = \beta_d\frac{\sqrt{-(r-r_1)(r-r_2)}}{2}$ (Eq. 15). With the values in Table 1, we estimate $\tilde{n}_{ch} \approx 2.9$, $\hat{\alpha}'_0 \approx 1.37$, $r_1 \approx 0.05$ and $r_2 \approx 18$. The range $\beta_d\frac{1+\hat{K}_{ex}}{\hat{K}_{ex}}r_1 < \mu_{ca} < \beta_d\frac{1+\hat{K}_{ex}}{\hat{K}_{ex}}r_2$ for μ_{ca} where oscillations occur increases as a function of $\tilde{n}_{ch}\hat{\alpha}'_0$ (Fig. 6A; cone (black curve) and rod (red curve)). It is much wider for a cone because of the larger β_d (Fig. 6A). No oscillations occur for Gcaps$^{-/-}$ mutants with $\tilde{n}_{ch}\hat{\alpha}'_0 = 0$. The oscillation frequency ω as function of μ_{ca} increases from zero towards the maximal frequency $\omega_{max} \approx \beta_d\frac{r_2}{4}$ attained for $r \approx \frac{r_2}{2}$ and $\mu_{ca} \approx \beta_d\frac{r_2}{2}$, and then decreases towards zero as μ_{ca} is further increased (Fig. 6B).

Although oscillations occur over a wide range of μ_{ca} values, they affect the recovery phase only if the damping rate is sufficiently small. For large μ_{ca} oscillations are damped and do not affect the recovery phase (Fig. 5A. magenta curve). As μ_{ca} decreases, the damping becomes smaller and oscillations start to appear during the recovery phase (Fig. 5C,D). It is difficult to give a precise value for μ_{ca} that marks when this happens. We note that for large μ_{ca} the current component $\hat{i}_{spr}$

in Eq. 14 decays with rate $\beta_d(1+\tilde{n}_{ch}\hat{\alpha}_0')$ (see analysis after Eq. 14). We reason that oscillations will become visible if μ_{damp} becomes smaller than this decay rate. Thus, from $\mu_{damp} \lesssim \beta_d(1+\tilde{n}_{ch}\hat{\alpha}_0')$ we estimate $\mu_{ca} \lesssim \beta_d(1+2\tilde{n}_{ch}\hat{\alpha}_0') = \beta_d \frac{r_1+r_2}{2} \sim 9\beta_d$, which is roughly compatible with Fig. 3A-B.

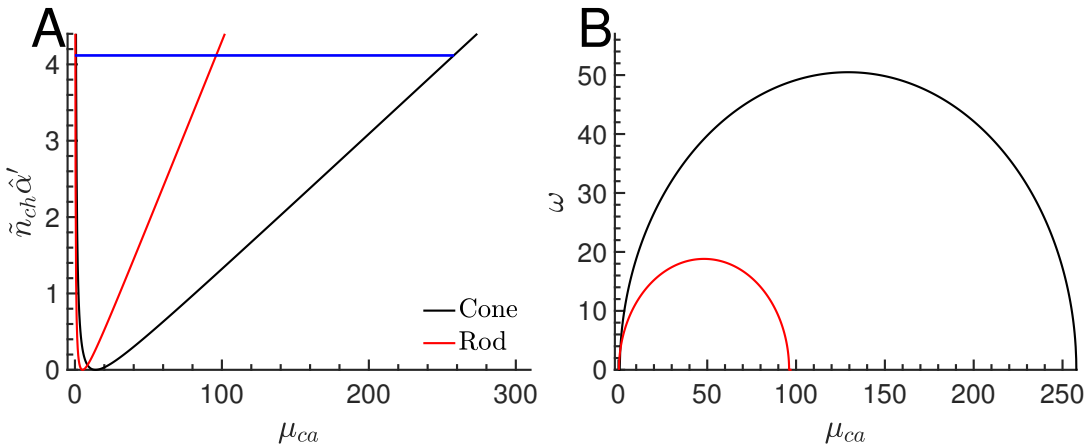

Figure 6: **Phase space for Ca^{2+} oscillations**. (A) Range for μ_{ca} where oscillations occur as a function of $\tilde{n}_{ch}\hat{\alpha}_0'$ for rod (red) and cone (back). The blue horizontal line indicates the value $\tilde{n}_{ch}\hat{\alpha}_0' \approx 4$ obtained with parameters from Table 1. (B) Oscillation frequency ω as a function of μ_{ca} for rod and cone.

Impact of changing the extracellular Ca^{2+} concentration

Finally, motivated by the experiments from [14], we investigated how changing in the extracellular Ca^{2+} concentration affects the light response. Assuming that Ca^{2+} influx through CNG channels is proportional to the extracellular Ca^{2+}-concentration, we compute that changing the extracellular concentration by a factor of $r_{ca,ex}$ alters the fraction of the CNG current carried by Ca^{2+} from the value $f_{ch,ca}$ to the new value $f'_{ch,ca} = f_{ch,ca}\frac{r_{ca,ex}}{1+(r_{ca,ex}-1)f_{ch,ca}}$ (see Materials and Methods for details). The altered Ca^{2+} influx modifies the dark steady-state values for Ca^{2+} and cGMP concentration, and the dark current. For $K_{ex} \gg c_{ca}$ we have that the exchanger current I_{ex} is proportional to c_{ca}, and therefore the ratio $I_{ex,d}/c_{ca,d}$ remains largely unaffected by changing extracellular Ca^{2+}. Moreover, with recoverin as main buffer we have $K_{ca,b} \gg c_{ca,d}$ (see Table 1), such that $B_{ca} = \frac{c_{ca,b,tot}K_{ca,b}}{(c_{ca,0}+K_{ca,b})^2}$ is only little modified by changes in the dark Ca^{2+} concentration. Thus, the rate μ_{ca} (Eq. 4) is only little unaffected by changing the extracellular Ca^{2+} concentration.

To illustrate the effect of changing extracellular Ca^{2+}, we investigated how the single-photon response in a cone is altered when the extracellular Ca^{2+} concentration is reduced by a factor of 10 (Fig. 7). With $r_{ca,ex} = 0.1$, the fraction of the CNG current carried by Ca^{2+} is reduced from $f_{ch,ca} = 0.3$ (Table 1) to $f'_{ch,ca} \approx 0.04$. This leads to a reduced dark Ca^{2+} concentration $\hat{c}_{ca,d} \approx 0.5$, which activates the cyclase and results in a higher dark cGMP concentration $\hat{c}_{cg,d} \approx 2.3$, and a larger dark current $\hat{I}_d \approx 3.7$ (see Materials and Methods). Because $\hat{K}_\alpha$ is larger with reduced dark Ca^{2+} concentration, it follows that the cyclase feedback $\hat{\alpha}_0'$ (see Eq. 9) is reduced from $\hat{\alpha}_0' \approx 1.37$ to $\hat{\alpha}_0' \approx 1$. To show the combined effect of these modifications, we compare the dimensional SPRs obtained by multiplying the normalized SPR from Fig. 3A with the dark current $I_d = 15pA$ (Fig. 7A, solid lines) to the SPRs computed with 10-fold reduced extracellular Ca^{2+} (Fig. 7A, dashed lines).

The larger SPR amplitude with reduced extracellular Ca^{2+} is mainly because of the 3.7 times larger dark current. Because of the smaller value of $\hat{\alpha}_0'$, the duration of the SPR becomes prolonged as for GCAPs$^{-/-}$ responses with $\hat{\alpha}_0' = 0$. The amplitude of the oscillation is reduced (Fig. 7B), since a lower $\hat{\alpha}_0'$ reduces the range for oscillations (Fig. 6A). These results are in agreement with the observations for a ten-fold decrease in extracellular Ca^{2+} concentration in primate cones [14].

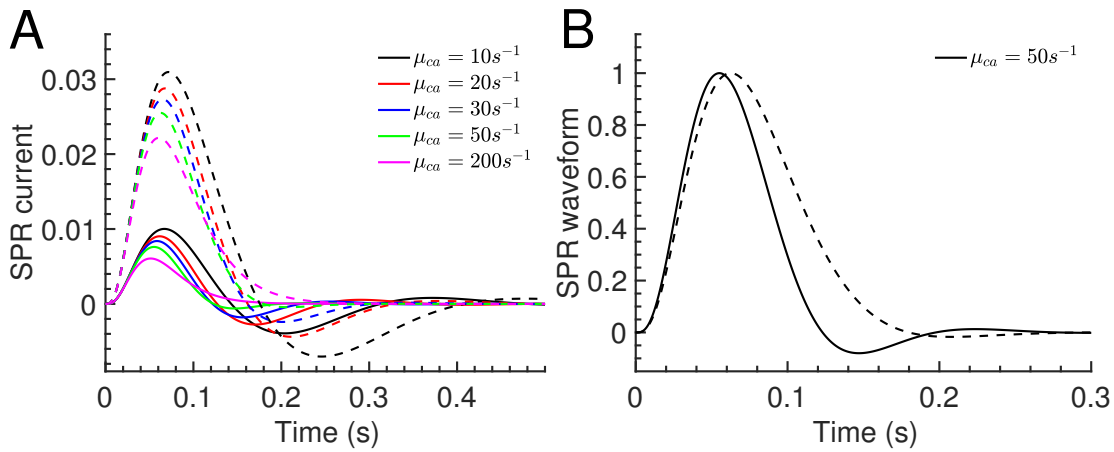

Figure 7: **Cone SPR with 10-fold reduced extracellular Ca^{2+} concentration.** (A) The solid lines show the cone SPR current with normal extracellular Ca^{2+} obtained by multiplying $\hat{i}_{spr}$ from Fig. 3A with the dark current $I_d = 15pA$. The dashed lines show the corresponding SPR with 10-fold reduced extracellular Ca^{2+}. (B) Comparison of the waveforms from (A) for $\mu_{ca} = 50s^{-1}$.

Discussion

The signal transduction pathway of rod and cone photoreceptors consists of a cascade of biophysical processes that transform light into a current response. Since many of these steps depend on Ca^{2+} feedback, it is important to understand how the dynamics of the free Ca^{2+} concentration affects the photoresponse. In previous work, we analysed the dim-light response assuming that the free Ca^{2+} concentration changes in proportion to the current [15, 16]. In this present work, we generalized our previous results by considering the effect of buffering, which can delay the Ca^{2+} dynamics with respect to the current.

We show that the dynamics of the free Ca^{2+} concentration is determined by the effective rate $\mu_{ca} = \frac{I_{ex,d}}{(1+B_{ca})F_A V_{os} c_{ca,d}}$ (see Eq. 4), where B_{ca} is the overall buffering constant in darkness, V_{os} is the outer segment volume, $I_{ex,d}$ is the exchanger current in darkness, $c_{ca,d}$ is the dark Ca^{2+} concentration, and F_A is the Faraday constant. Whereas more buffering decreases μ_{ca} and slows down the Ca^{2+} dynamics, a smaller OS volume and a larger basal Ca^{2+} exchange rate characterised by a higher current $I_{ex,d}$ speeds up the dynamics. For large μ_{ca} (the time scale μ_{ca}^{-1} is small compared to the time scale of the current change), the Ca^{2+} and current dynamics become tightly coupled and the Ca^{2+} concentration changes in proportion to the current. As μ_{ca} decreases, for example due to increased buffering, the Ca^{2+} concentration becomes more and more delayed with respect to the current (Fig. 4C-D), and eventually oscillations emerge (Fig. 4A-B). Since we considered only fast buffers, this shows that current oscillations are not necessarily an indication for the presence of slow buffers.

Recoverin is the most abundant calcium buffer in the outer segment [4, 26], with a dissociation constant $K_{ca,rec} \sim 3\mu M$ for the reaction between free Ca^{2+} and recoverin [27]. With $B_{ca} \sim 50$ estimated for a mouse rod [24], we compute that the recoverin concentration in the OS would have to be around $c_{rec} \sim B_{ca}K_{ca,rec} \sim 150\mu M$. Such a value is consistent with estimations from [10], but it is much larger than $c_{rec} \sim 26\mu M$ found for a carp rod [26]. In contrast, a GCAPs concentration around $c_{gcaps} \sim 3\mu M$ with a dissociation constant $K_{ca,gcaps} \sim 0.14\mu M$ contributes to the rod buffering constant in darkness only a value around $3 \times 0.14/(0.3 + 0.14)^2 \sim 2$. With $B_{ca} = 50$ and Table 1, we compute $\mu_{ca} \approx 32s^{-1}$ for a mouse rod, and $\mu_{ca} \approx 184s^{-1}$ for a cone. Such values lead to monophasic flash responses (Fig. 3), in agreement with experimental recordings [15, 28]. A larger value of μ_{ca} for cones is consistent with a faster response dynamics in cones compared to rods. However, since the concentration of recoverin is much higher in cones that in rods [26], the buffering constant B_{ca} is likely to be larger in cones than in rods. Since $K_{ca,rec} \sim 3\mu M$ is much larger than the Ca^{2+} concentration in darkness around $0.3\mu m$ (Table. 1), it follows that the buffering constant B_{ca} does not much increase as the Ca^{2+} concentration further decreases with light. This ensures that μ_{ca} does not decrease, and dynamics of the Ca^{2+} concentration remain fast as the light intensity increases.

Our analytic results reveal that the expression for the dim-light response is a sum of exponentials (Eq. 14). The various exponential decay rates reflect the decay rates of the biophysical processes that contribute to PDE activation, and the interaction between cGMP and Ca^{2+} via feedback to the cyclase. The phase space for the interaction between cGMP and Ca^{2+} depends on the ratio $r \sim \mu_{ca}/\beta_d$ (Fig. 6). If the Ca^{2+} dynamics are fast such that r is sufficiently large ($r \gtrsim 1+2\tilde{n}_{ch}\hat{\alpha}'_0 \sim 9$), the recovery phases of flash responses are monophasic (Fig. 3A-B), and the Ca^{2+} concentration changes in proportion to the current (Fig. 4C). For slower Ca^{2+} dynamics ($r \lesssim 1 + 2\tilde{n}_{ch}\hat{\alpha}'_0$), damped oscillations emerge (Fig. 4A), and the Ca^{2+} concentration becomes more and more delayed with respect to the current (Fig. 4C). Oscillations are also visible during initial and recovery phases of step responses (Fig. 4B). The Ca^{2+} dynamics does not affect the intermediate plateau value of step responses, because this is determined by steady-state properties. Whereas the rising and recovery phases of flash responses have different shapes, there is a symmetry between the initial and recovery phases of step responses (Fig. 4B); see also Fig. 5B in [29]). Hence, the analysis of initial and recovery phase of dim step responses gives similar information, whereas complementary information can be extracted for flash responses [16].

We find that changing the Ca^{2+} dynamics affects the light response primarily via the feedback to the cyclase (Fig. 3). For GCAPs$^{-/-}$ photoreceptors where the cyclase is not Ca^{2+}-dependent, the current depends only very little on the value of μ_{ca}. For WT rods or cones, modifying μ_{ca} affects amplitude and the shape of flash responses (Fig. 3A-B, Fig. 4A-B). The amplitude of the single-photon response (SPR) increases with slower Ca^{2+} dynamics because the negative feedback to the cyclase is delayed. The maximum value for the ratio between the SPR amplitude of a GCAPs$^{-/-}$ and WT photoreceptor is around 2-3, which is achieved with fast Ca^{2+} dynamics where the Ca^{2+} concentration changes in proportion to the current. Since such maximal ratios are observed experimentally [15, 8, 30], this suggests that under normal physiological conditions the dynamics of the Ca^{2+} concentration in rods and cones is determined by the current.

Although oscillations might not occur under physiological conditions, they have been observed after the application of the Ca^{2+} buffer BAPTA in primate and guinea pig rods [7, 8, 9], mouse rods [8, 10], and toad rods [9]. In primate cones, oscillations have been observed occasionally even without any treatment [11, 12, 13]. Because oscillations occur if the ratio μ_{ca}/β_d is sufficiently small, we speculate that they have been observed in cones without BAPTA treatment because of the larger value of β_d. Recently it has been claimed that primate cones have predominantly monophasic responses [14], and biphasic responses may have been the result of experimental conditions [14]. Accordingly, it has been

shown that a biphasic cone response could be transformed into a monophasic response by lowering the extracellular Ca^{2+} concentration (see Fig. 2A in [14]). The reduced extracellular Ca^{2+} concentration also prolonged the flash response and increased the peak amplitude by a factor of around 3-4 (such effects have also been observed for rods treated with BAPTA [7]). Our analysis with tenfold reduced extracellular Ca^{2+} concentration provides a theoretical explanation for these observations (Fig. 7): reducing extracellular Ca^{2+} increases the flash amplitude, prolongs the response, and reduces the undershoot (Fig. 7).

In order to keep the analysis comprehensible, we did not include slow buffers in this work. The impact of slow buffering can be studied by including additional equations for Ca^{2+} interacting with slow buffers. For example, in first approximation, and with a single slow buffer, Eq. 8 will be replaced by 3-dimensional system of linear equations. Although the phase space will be more complex, we do not expect to find solutions that are qualitatively very different from what we observed here.

In this work we used a spatially well-stirred model in order to obtain analytic results that provided conceptual insight. Such models are frequently used to analyse the photoresponse [15, 31, 18, 25, 22, 23, 21, 32, 4]. Whereas spatial models are a more accurate description of reality [17, 33, 19, 20, 34], the downside is that no analytic results can usually be derived. However, such results are extremely important because they provide a conceptual understanding that subsequently can be refined using spatial simulations. We used our spatially resolved phototransduction model [19] to perform simulations that showed that our conclusions remain valid when using a spatially resolved model (not shown). Recently, it has been found that the large outer segment of frog rods is a spatially inhomogeneous compartment [6, 35]. However, no such findings exist for mouse or primate rods and cones, which we focused on in this work. Moreover, it is unclear whether a relevant inhomogeneity exists in these photoreceptors, because their outer segment is much smaller compared to a frog rod [4]. Finally, even with an inhomogeneous OS, we still expect that the results and conclusion derived here remain valid in first approximation.

Although we focused on the dim-light response in darkness, the first order analysis that we outlined can be generalized to study the light response also in presence of a background light. In this case one has to first numerically compute the steady-state values for the background light, and then apply the linearisation procedure with parameters that have been normalized with the steady state values corresponding to the background light.

Author contributions

AA performed analysis and generated figures. JR designed the research, performed analysis and wrote the manuscript.

Acknowledgements

We are grateful to Gordon Fain for comments and careful reading of the manuscript. This work was funded by a grant from Agence Nationale de Recherche (ANR) to JR.

Parameter	Description	Rod	Cone
ξ	Gain of PDE activation	0.18[15]	0.0007 [15]
β_d (s^{-1})	Dark turnover rate	4.1 [15]	11 [15]
μ_{rh} (s^{-1})	Deactivation rate of activated photopigment	28 [15]	70 [15]
μ_{pde} (s^{-1})	Deactivation rate of activated PDE	5[15]	37.8[15]
μ_{tr} (s^{-1})	Deactivation rate of activated transducin	23.8 [15]	71 [15]
K_{ex} (μM)	Sensitivity of NCKX exchanger to Ca^{2+}	1.6 [4]	1.6
K_{ch} (μM)	Sensitivity of CNG channels to cGMP	20 [4]	20
n_{ch}	CNG channel cooperativity	2.5 [15]	2.5 [15]
K_α (μM)	Cyclase affinity to Ca^{2+}	0.14 [36, 26]	0.14
r_α	Ratio of minimal to maximal cyclase activity	1/30 [37, 36]	1/30
n_α	Hill coefficient for the cyclase	2 [15]	2 [15]
$f_{ch,ca}$	Fraction of the CNG current carried by Ca^{2+}	0.12 [20]	0.3 [38]
I_0 (pA)	Dark current	15 [15]	15 [15]
$c_{ca,0}$ (μM)	Dark Ca^{2+} concentration	0.3 [15]	0.3 [15]
$c_{cg,0}$ (μM)	Dark cGMP concentration	4 [15]	4 [15]
V_{os} (μm^3)	Outer segment volume	18 [19]	18/2.5 [39, 28]
$K_{ca,b}$ (μM)	Ca^{2+} affinity for recoverin buffering	3 [27]	3

Table 1: Parameter values for mouse rods and cones.

References

[1] M. E. Burns and E. N. Pugh Jr, "Lessons from photoreceptors: turning off g-protein signaling in living cells," *Physiology*, vol. 25, no. 2, pp. 72–84, 2010.

[2] V. Arshavsky and M. Burns, "Photoreceptor signaling: supporting vision across a wide range of light intensities.," *J Biol Chem*, vol. 287, pp. 1620–1626, 2012.

[3] V. Arshavsky, T. Lamb, and E. Pugh Jr, "G proteins and phototransduction," *Annu. Rev. Physiol.*, vol. 64, pp. 153–187, 2002.

[4] E. Pugh Jr and T. Lamb, "Phototransduction in vertebrate rods and cones: Molecular mechanism of amplification, recovery and light adaptation," *In Handbook of Biological Physics Vol. 3, Elsevier Science B. V., Amsterdam*, pp. 183–255, 2000.

[5] F. Vinberg, J. Chen, and V. Kefalov, "Regulation of calcium homeostasis in the outer segments of rod and cone photoreceptors.," *Prog Retin Eye Res.*, vol. 67, pp. 87–101, 2018.

[6] Y. Li, F. Falleroni, S. Mortal, U. Bocchero, D. Cojoc, and V. Torre, "Calcium flares and compartmentalization in rod photoreceptors," *Proceedings of the National Academy of Sciences*, vol. 117, no. 35, pp. 21701–21710, 2020.

[7] G. Field and F. Rieke, "Mechanisms regulating variability of the single-photon responses of mammalian rod photoreceptors," *Neuron*, vol. 35, pp. 733–747, 2002.

[8] M. E. Burns, A. Mendez, J. Chen, and D. A. Baylor, "Dynamics of cyclic gmp synthesis in retinal rods.," *Neuron.*, vol. 36, pp. 81–91, 2002.

[9] F. Rieke and D. Baylor, "Origin of reproducibility in the responses of retinal rods to single photons," *Biophys. J.*, vol. 75, pp. 1836–1857, 1998.

[10] C. L. Makino, R. Dodd, J. Chen, M. E. Burns, A. Roca, M. Simon, and D. Baylor, "Recoverin regulates light-dependent phosphodiesterase activity in retinal rods," *The Journal of general physiology*, vol. 123, no. 6, pp. 729–741, 2004.

[11] D. Schneeweis and J. Schnapf, "The photovoltage of macaque cone photoreceptors: adaptation, noise, and kinetics.," *J Neurosci.*, vol. 19, pp. 1203–16, 1999.

[12] J. Schnapf, B. Nunn, M. Meister, and D. Baylor, "Visual transduction in cones of the monkey macaca fascicularis," *J. Physiol.*, vol. 427, pp. 681–713, 1990.

[13] D. Baylor, B. Nunn, and J. Schnapf, "Spectral sensitivity of cones of the monkey macaca fascicularis.," *The Journal of Physiology*, vol. 390, no. 1, pp. 145–160, 1987.

[14] L.-H. Cao, D.-G. Luo, and K.-W. Yau, "Light responses of primate and other mammalian cones," *Proceedings of the National Academy of Sciences*, vol. 111, no. 7, pp. 2752–2757, 2014.

[15] J. Reingruber, N. Ingram, K. Griffis, and G. Fain, "A kinetic analysis of mouse rod and cone photoreceptor responses.," *J Physiology*, vol. 598, no. 17, pp. 3747–63, 2020.

[16] A. Abtout, G. Fain, and J. Reingruber, "Analysis of waveform and amplitude of mouse rod and cone flash responses.," *The Journal of Physiology*, vol. 599, no. 13, pp. 3295–3312, 2021.

[17] C. Klaus, G. Caruso, V. V. Gurevich, H. E. Hamm, C. L. Makino, and E. DiBenedetto, "Phototransduction in retinal cones: Analysis of parameter importance," *PloS one*, vol. 16, no. 10, p. e0258721, 2021.

[18] L. Astakhova, M. Firsov, and V. Govardovskii, "Activation and quenching of the phototransduction cascade in retinal cones as inferred from electrophysiology and mathematical modeling," *Molecular vision*, vol. 21, p. 244, 2015.

[19] J. Reingruber, J. Pahlberg, M. Woodruff, A. Sampath, G. Fain, and D. Holcman, "Detection of single photons by rod photoreceptors," *Proc Natl Acad Sci U S A*, vol. 110, no. 48, pp. 19378–83, 2013.

[20] O. Gross, E. N. Pugh, and M. Burns, "Spatiotemporal cgmp dynamics in living mouse rods.," *Biophys. J.*, vol. 102, no. 8, pp. 1775–1784, 2012.

[21] R. Hamer, S. Nicholas, D. Tranchina, T. Lamb, and J. Jarvinen, "Toward a unified model of vertebrate rod phototransduction," *Vis. Neurosci.*, vol. 22, pp. 417–436, 2005.

[22] J. Korenbrot, "Speed, adaptation, and stability of the response to light in cone photoreceptors: the functional role of ca-dependent modulation of ligand sensitivity in cgmp-gated ion channels.," *J Gen Physiol*, vol. 139, no. 1, pp. 31–56, 2012.

[23] J. Chen, M. Woodruff, T. Wang, F. Concepcion, D. Tranchina, and G. Fain, "Channel modulation and the mechanism of light adaptation in mouse rods.," *J Neurosci*, vol. 30, no. 48, pp. 16232–16240, 2010.

[24] O. Gross, E. N. Pugh, and M. Burns, "Calcium feedback to cgmp synthesis strongly attenuates single-photon responses driven by long rhodopsin lifetimes.," *Neuron*, vol. 76, no. 2, pp. 370–82, 2012.

[25] B. M. Invergo, D. Dell'Orco, L. Montanucci, K.-W. Koch, and J. Bertranpetit, "A comprehensive model of the phototransduction cascade in mouse rod cells," *Molecular bioSystems*, vol. 10, no. 6, pp. 1481–1489, 2014.

[26] S. Kawamura and S. Tachibanaki, "Molecular basis of rod and cone differences," *Progress in retinal and eye research*, p. 101040, 2021.

[27] C.-K. Chen, J. Inglese, R. J. Lefkowitz, and J. B. Hurley, "Ca2+-dependent interaction of recoverin with rhodopsin kinase," *Journal of Biological Chemistry*, vol. 270, no. 30, pp. 18060–18066, 1995.

[28] N. Ingram, A. Sampath, and G. Fain, "Why are rods more sensitive than cones?," *J Physiol*, vol. 594, no. 19, pp. 5415–26, 2016.

[29] N. Ingram, A. Sampath, and G. Fain, "Voltage-clamp recordings of light responses from wi and mutant mouse cone photoreceptors.," *J Gen Physiol*, vol. 151, no. 11, pp. 1287–1299, 2019.

[30] A. Mendez, M. Burns, I. Sokal, A. Dizhoor, W. Baehr, K. Palczewski, D. Baylor, and J. Chen, "Role of guanylate cyclase-activating proteins (gcaps) in setting the flash sensitivity of rod photoreceptors.," *Proc Natl Acad Sci U S A*, vol. 98, pp. 9948–9953, 2001.

[31] C. J. Beelen, S. Asteriti, L. Cangiano, K.-W. Koch, and D. Dell'Orco, "A hybrid stochastic/deterministic model of single photon response and light adaptation in mouse rods," *Computational and Structural Biotechnology Journal*, vol. 19, pp. 3720–3734, 2021.

[32] R. Hamer, S. Nicholas, D. Tranchina, P. Liebman, and T. Lamb, "Multiple steps of phosphorylation of activated rhodopsin can account for the reproducibility of vertebrate rod single-photon responses," *J. Gen. Physiol.*, vol. 122, pp. 419–444, 2003.

[33] T. D. Lamb and T. W. Kraft, "Quantitative modeling of the molecular steps underlying shut-off of rhodopsin activity in rod phototransduction," *Molecular vision*, vol. 22, p. 674, 2016.

[34] P. Bisegna, G. Caruso, D. Andreucci, L. Shen, V. Gurevich, H. Hamm, and E. DiBenedetto, "Diffusion of the second messengers in the cytoplasm acts as a variability suppressor of the single photon response in vertebrate phototransduction," *Biophys. J.*, vol. 94, pp. 3363–3383, 2008.

[35] M. Mazzolini, G. Facchetti, L. Andolfi, R. P. Zaccaria, S. Tuccio, J. Treu, C. Altafini, E. M. Di Fabrizio, M. Lazzarino, G. Rapp, *et al.*, "The phototransduction machinery in the rod outer segment has a strong efficacy gradient," *Proceedings of the National Academy of Sciences*, vol. 112, no. 20, pp. E2715–E2724, 2015.

[36] I. Peshenko, E. Olshevskaya, A. Savchenko, S. Karan, P. K, W. Baehr, and A. Dizhoor, "Enzymatic properties and regulation of the native isozymes of retinal membrane guanylyl cyclase (retgc) from mouse photoreceptors.," *Biochemistry*, vol. 50, no. 25, pp. 5590–600, 2011.

[37] I. Peshenko and A. Dizhoor, "Ca2+ and mg2+ binding properties of gcap-1. evidence that mg2+-bound form is the physiological activator of photoreceptor guanylyl cyclase.," *J Biol Chem.*, vol. 281, no. 33, pp. 23830–41, 2006.

[38] T. Ohyama, D. H. Hackos, S. Frings, V. Hagen, U. B. Kaupp, and J. I. Korenbrot, "Fraction of the dark current carried by ca2+ through cgmp-gated ion channels of intact rod and cone photoreceptors," *The Journal of general physiology*, vol. 116, no. 6, pp. 735–754, 2000.

[39] S. Nikonov, R. Kholodenko, J. Lem, and E. Pugh Jr, "Physiological features of the s- and m-cone photoreceptors of wild-type mice from single-cell recordings.," *J Gen Physiol*, vol. 127, no. 4, pp. 359–74, 2006.